
Proceedings Paper:
Houghton, M orcid.org/0000-0003-3244-5699, Head, D orcid.org/0000-0003-0216-6787 and Walkley, M orcid.org/0000-0003-2541-4173 (2019) A Numerical Model for Random Fibre Networks. In: Nikolov, G, Kolkovska, N and Georgiev, K, (eds.) Lecture Notes in Computer Science. 9th International Conference on Numerical Methods and Applications (NMA 2018), 20-24 Aug 2018, Borovets, Bulgaria. Springer , pp. 408-415. ISBN 978-3-030-10691-1

https://doi.org/10.1007/978-3-030-10692-8_46

A Numerical Model For Random Fibre Networks

Mark Houghton*[0000−0003−3244−5699], David Head[0000−0003−0216−6787], and Mark Walkley[0000−0003−2541−4173]

University Of Leeds, Leeds, UK

Abstract. Modelling a random fibre network representative of a real world material leads to a large sparse linear matrix system with a high condition number. Current off-lattice networks are not a realistic model for the mechanical properties of the large volume of random fibres seen in actual materials. In this paper, we present the numerical methods employed within our two-dimensional and three-dimensional models that improve the computational time limitations seen in existing off-lattice models. Specifically, we give a performance comparison of two-dimensional random fibre networks solved iteratively with different choices of preconditioner, followed by some initial results of our three-dimensional model.

Keywords: Fibre network · Iterative · Preconditioning.

1 Introduction

Many real world materials can be represented at the microscopic level by a random network of fibres, including paper and felt, non-woven fabrics, tissue scaffolds, and the cytoskeletons of eukaryotic cells. A good understanding of the mechanical behaviour of these networks is key to understanding physical properties at the macroscopic level and for the development of new materials.

2 Modelling a Random Fibre Network

In many applications, especially biological, it is appropriate to model individual fibres as semiflexible polymers [5]. With this assumption in place, the extensible *Wormlike Chain* model has been shown to adequately describe the elastic behaviour of individual semiflexible fibres [6]. Discretising this we can define fibre stretching, compression and bending, but we choose to neglect thermal contributions for simplicity. To expand this theory from single fibres to whole networks we adopt the Mikado model [3, 4, 7], which allows us to express the energy of the system as the total sum of stretching energy added to the total sum of bending energy of the network,

$$E = \frac{\mu}{2} \sum_{ij} \frac{\delta \ell_{ij}^2}{\ell_{ij}} + \frac{1}{2} \sum_{\langle ijk \rangle} \frac{\kappa_{ijk} \theta_{ijk}^2}{\bar{\ell}_{ijk}}, \tag{1}$$

* Supported by an EPSRC (UK) DTP studentship.

where the left sum considers all segments, ij, of every fibre of the network, and the right sum considers all of the consecutive segments, ij, jk, along each fibre, for stretching constant μ, bending modulus κ_{ijk}, segment length ℓ_{ij}, average length of two consecutive segments $\bar{\ell}_{ijk}$, and angular deflection θ_{ijk}. To better understand (1), it is useful to first consider individual fibres.

2.1 Fundamentals

Defining fibres as slender elastic bodies with uniform circular cross-sections, we can consider a two-dimensional plane or three-dimensional cuboid wherein a predetermined number of fibres are generated with random position and orientation. After cross-linking these fibres (see 2.5), a mechanical structure remains in which nodes are identified as freely rotating points, and categorised as one of three types. Boundary nodes occur as points fixed at the aperiodic boundaries of the domain, dangling nodes are attributed to the end points of fibres not on the boundary, and internal nodes are the points associated with cross-links. For adjacent nodes φ,ψ the tangent vector along the segment is

$$\hat{\mathbf{t}}_{\varphi\psi} = \frac{\mathbf{s}_\psi - \mathbf{s}_\varphi}{\ell_{\varphi\psi}},$$

where $\mathbf{s}_\varphi$ is the position vector at φ and $\ell_{\varphi\psi} = |\mathbf{s}_\psi - \mathbf{s}_\varphi|$ is the segment length. We denote $\mathbf{u}_\varphi$ as the displacement of an individual node after a load or perturbation has been applied to the network, and refer to individual components as $u_{\varphi_x}, u_{\varphi_y}, u_{\varphi_z}$.

2.2 Local Stretching Behaviour

Consider a segment $\varphi\psi$ comprising of an adjacent node pair φ, ψ respectively, treated as a simple Hookean spring. The stretching energy for this segment is

$$E^{\text{stretch}}_{\varphi\psi} = \frac{k_{\varphi\psi}}{2}[(\mathbf{u}_\psi - \mathbf{u}_\varphi)\cdot\hat{\mathbf{t}}_{\varphi\psi}]^2$$

with a stretching constant $k_{\varphi\psi} = \frac{\mu}{\ell_{\varphi\psi}} = \frac{AE^f}{\ell_{\varphi\psi}}$, for $A = \pi r^2$, radius r and Young's modulus E^f. The second partial derivatives of this energy contribute to the global Hessian matrix at rows and columns corresponding to the displacements of φ and ψ, and the first partial derivatives contribute to the right hand side vector.

2.3 Local Bending Behaviour

For the adjacent node triplet α, ω, β, segment $\alpha\omega\beta$ has bending energy

$$E^{\text{bend}}_{\alpha\omega\beta} = \frac{\kappa_{\alpha\omega\beta}\theta^2_{\alpha\omega\beta}}{2\bar{\ell}_{\alpha\omega\beta}} = \frac{\kappa_{\alpha\omega\beta}\left[(\mathbf{s}_\omega - \mathbf{s}_\alpha)\times(\mathbf{u}_\beta - \mathbf{u}_\omega) + (\mathbf{u}_\omega - \mathbf{u}_\alpha)\times(\mathbf{s}_\beta - \mathbf{s}_\omega)\right]^2}{\ell^2_{\alpha\omega}\ell^2_{\omega\beta}(\ell_{\alpha\omega} + \ell_{\omega\beta})},$$

for a bending constant $\kappa_{\alpha\omega\beta} = \frac{AE^f r^2}{4}$, with $A = \pi r^2$ and Young's modulus E^f. Similar to the stretching case, local contributions to the global Hessian and right hand side vector can be derived from this energy.

2.4 Global Assembly

Combining the displacements $\mathbf{u}_\varphi$ of every node φ, in the vector $\mathbf{U}$,

$$\mathbf{U} = [U_1, U_2, U_3, U_4, ...] = [u_{1_x}, u_{2_x}, ..., u_{1_y}, u_{2_y}, ..., u_{1_z}, u_{2_z}, ...],$$

then a Taylor series expansion of the energy of the system about $\mathbf{U} = 0$ is

$$E(\mathbf{U}) = E_0 + \sum_{i=1}^{N} U_i \frac{\partial E}{\partial U_i}\bigg|_{\mathbf{U}=\mathbf{0}} + \frac{1}{2}\sum_{i=1}^{N}\sum_{j=1}^{N} U_i U_j \frac{\partial^2 E}{\partial U_i \partial U_j}\bigg|_{\mathbf{U}=\mathbf{0}} + \ ...$$

The resulting system represents the network in mechanical equilibrium with the applied load or perturbation;

$$\sum_j U_j \frac{\partial^2 E}{\partial U_i \partial U_j} = B_i, \quad \text{where } B_i = -\frac{\partial E}{\partial U_i}\bigg|_{\mathbf{U}=\mathbf{0}}$$

for $i, j = 1, ..., N$. Denoting the Hessian matrix as H, this gives the global linear matrix system $H\mathbf{U} = \mathbf{B}$ which can be assembled from the local contributions defined in sections 2.2 and 2.3.

2.5 Cross-linking Fibres

In a two dimensional plane, a pair of randomly orientated fibres are trivially cross-linked at their unique point of intersection, if this exists. In three dimensions direct intersections of randomly orientated fibres occur with probability zero for radius, $r \to 0^+$. In this case, the minimum separation is considered, and if this is below a given threshold, a short cross-linking fibre is inserted between the two closest points of the original pair of fibres. The cross-linking fibre can either be treated as a stiff and non-rotating inextensible rod, in which case each end point displaces identically, or as an elastic spring, in which case each end point can displace individually. An alternative approach is to constrain fibre orientation to lie along lattice vectors, such that fibres directly intersect. This lattice-based approach can achieve mechanical rigidity at lower fibre counts due to the higher coordination (connectivity) number, z_c, and has been used successfully to predict mechanical properties comparable to randomly orientated fibre networks seen in real-world materials [2]. We have made some preliminary lattice-based experiments (discussed in Section 4.3) before moving to randomly orientated networks.

3 Numerical Model

3.1 Linear System Structure (in 2D)

By grouping the unknown displacements in $\mathbf{U}$ by coordinate direction, the block structure of H can be written as

$$H = \begin{bmatrix} H_{xx} & H_{xy} \\ H_{xy}^T & H_{yy} \end{bmatrix}, \quad \text{where } H_{\varphi\psi} = \frac{\partial^2 E}{\partial u_{\varphi_i} \partial u_{\psi_j}}, \tag{2}$$

for $i, j = 1, ..., N$.

The sparsity of H is determined from the local connectivity of each fibre with the other fibres in the network. An initial estimate of the sparsity pattern can be obtained from the adjacency matrix of the internal nodes of a network, and is repeated for each sub-block $H_{\varphi\psi}$ of the global matrix H. To exploit the sparsity of H, we store the non-zero values in compressed sparse row (CSR) format. The matrix H is symmetric, as are each of the diagonal sub-blocks, but each off-diagonal sub-block is not necessarily symmetric.

3.2 Iterative Solution Strategy

Our system is symmetric but may not be positive definite, hence we choose the MINRES iterative method from the family of Krylov subspace methods. These methods perform best when the system is preconditioned to cluster the matrix eigenvalues. Exploiting the block structure seen in (2), we take the diagonal blocks

$$P_{Db} = \begin{bmatrix} H_{xx} & O \\ O & H_{yy} \end{bmatrix}, \tag{3}$$

as the first choice of preconditioner. A similar preconditioner can be defined when extending to three dimensions. Additionally we can also consider a simple asymmetric preconditioner and a symmetric preconditioner with a Schur complement block

$$P_{Ab} = \begin{bmatrix} H_{xx} & H_{xy} \\ O & H_{yy} \end{bmatrix}, \quad P_S = \begin{bmatrix} H_{xx} & O \\ O & S \end{bmatrix}, \tag{4}$$

where $S = H_{yy} - H_{xy}^T H_{yy}^{-1} H_{xy}$. GMRES was used with P_{Ab}, since this preconditioner does not preserve the symmetry of H.

4 Results

4.1 Performance Comparison in 2D

To evaluate the performance of the different choices of preconditioner, we measured the number of iterations required to converge to a relative tolerance of 10^{-3}, using the MINRES and GMRES solvers in MATLAB. The rate of convergence was measured for increasing system size by increasing the number of fibres, N_f, with fixed length $\ell = 0.25$ and radius $r = 0.01$. For each interval of N_f, the results were averaged over 10 reproducibly-seeded randomly generated networks. Examples of individual network generations with varying N_f can be seen in Figure 1.

As can be seen from Table 1, P_{Db} shows a consistent performance as N_f increases, with good evidence that we would expect to see the iteration number converge if N_f were to increase further. P_S also performs well, and P_{Ab} consistently shows the lowest iteration count for increasing N_f, but the additional cost in building the P_S preconditioner, and the additional cost per iteration of GMRES versus MINRES leaves P_{Db} as potentially the preferred choice. The

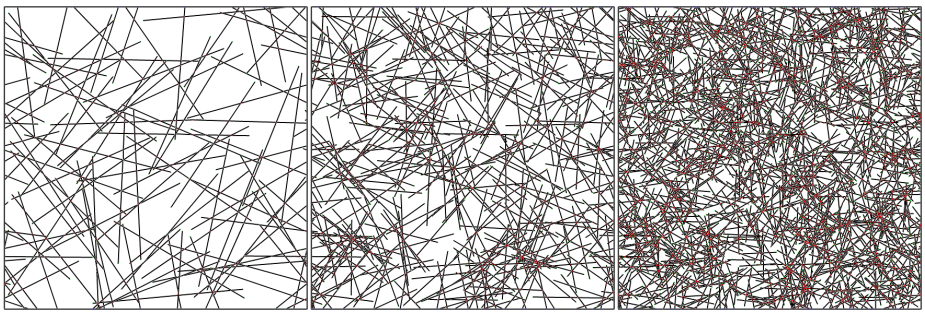

Fig. 1. Examples of generated 2D random fibre networks increasing in area with a fixed fibre density. The number of fibres, N_f, is 100 *(left)*, 400 and 1600 *(right)*, and fibre length, ℓ, and radius, r, are fixed at 0.25 and 0.01 respectively, but r is not to scale. Dangling ends have not been removed.

diagonally scaled preconditioner D performs the worst, with large fluctuations in the iteration count and a large standard error.

Table 1. Number of iterations required to converge for different preconditioners and an increasing number of fibres, N_f, of length 0.25 and radius 0.01. Standard error was calculated from a sample of 10 networks.

N_f	100	200	400	800
D	300.2 ± 54.0	480.8 ± 67.3	570.6 ± 77.3	410.9 ± 103.0
P_{Db}	8.0 ± 0.8	8.5 ± 0.5	7.7 ± 0.7	7.2 ± 0.6
P_S	12.3 ± 1.1	14.6 ± 1.2	13.8 ± 1.3	14.1 ± 0.9
P_{Ab}	5.3 ± 0.2	5.4 ± 0.2	5.4 ± 0.2	5.3 ± 0.2

As a further indication of performance we also collected estimates for the condition numbers of the preconditioned system and for H. To do this we consider a similar range of N_f as previously and provided the default seed to the `condest` function in MATLAB for 10 network generations at each interval. From the results in Table 2 we find additional evidence for the poor performance of D, with condition number estimates consistently higher than H without any preconditioning. P_S reduces the condition number of H by roughly an order of magnitude, and P_{Db} and P_{Ab} demonstrate the best performance, showing similar estimates to each other with the symmetric having slightly lower values on average for larger N_f.

In addition to analysing the performance of the preconditioners, we also investigated the mechanical properties of the networks. In particular for $N_f = 100$, with $\ell = 0.25$, we varied r and measured the shear modulus, G, and ratio of bending energy over total energy, E^b/E. From Figure 2 *(right)* we can see a smooth crossover from a regime with comparable stretching and bending ener-

Table 2. Estimated condition numbers, κ, of different preconditioners applied to H, for varied number of fibres, N_f.

N_f	100	200	400	800	1600
$\kappa(H)$	3.74e6	7.58e6	1.81e7	4.34e7	9.72e7
$\kappa(D^{-1}H)$	8.51e6	2.41e7	7.09e7	1.98e8	4.54e8
$\kappa(P_{Db}^{-1}H)$	7.32e4	1.47e5	4.85e5	1.60e6	5.12e6
$\kappa(P_{S}^{-1}H)$	1.39e5	4.97e5	1.18e6	4.22e6	-
$\kappa(P_{Ab}^{-1}H)$	6.98e4	1.96e5	5.99e5	2.11e6	-

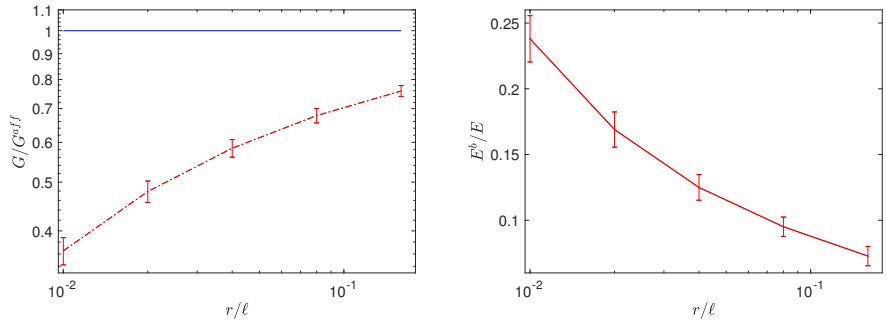

Fig. 2. r/ℓ, for $\ell = 0.25$ and $N_f = 100$ in a 0.5×0.5 plane against G/G^{aff} *(left)* and against E^b/E *(right)*. Nodes within a distance of 10^{-3} were merged into a single node prior to solution. The line $G/G^{\text{aff}} = 1$ *(left)* corresponding to affine response is also shown.

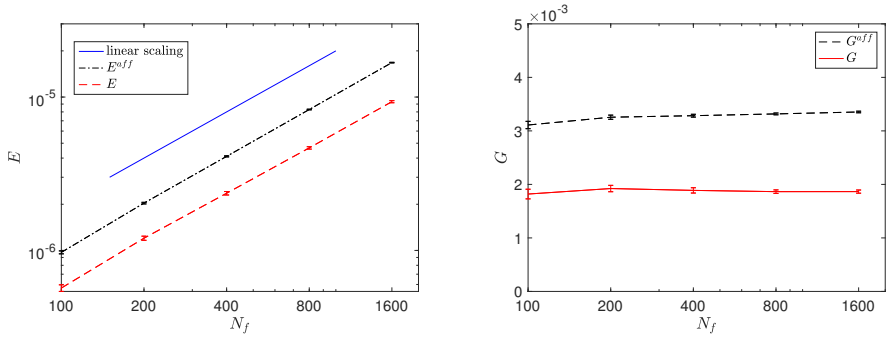

Fig. 3. Calculated values of the energy *(left)* and shear modulus *(right)* verified against the affine predictions for an increasing number of fibres with fixed length 0.25 and radius 0.01. The solid line is added to verify linear scaling.

gies for small r, to a stretching dominated regime for large r. Figure 2 *(left)* demonstrates a smooth transition between affine (i.e. uniform deformation field) dominated behaviour at large r to non-affine behaviour for small r. This coincides well with the known result that stretching-dominated networks become close to affine [4].

4.2 Validation

To validate our model results, we verified that the calculated energy, E, and shear modulus, G, were bounded by the affine predictions E^{aff} and G^{aff} respectively. To do this, we increased N_f for $\ell = 0.25$ and $r = 0.01$, and plotted E and G alongside their corresponding affine predictions. Figure 3 demonstrates that E *(left)* and G *(right)* lie below the limits provided by the affine predictions. We can also see that E increases linearly with N_f, as we would expect.

4.3 Preliminary Results in 3D

In a step towards solving randomly orientated three dimensional networks built from the Mikado approach, we were able to obtain preliminary results by solving networks with predetermined direct intersections between fibres. These have irregularity introduced by overlaying different lattice based components together to form a rigid structure. More specifically we take 25 vertical fibres extending the height of a $1 \times 1 \times 1$ cube and insert lattice forming plates through the vertical fibres with varied orientations.

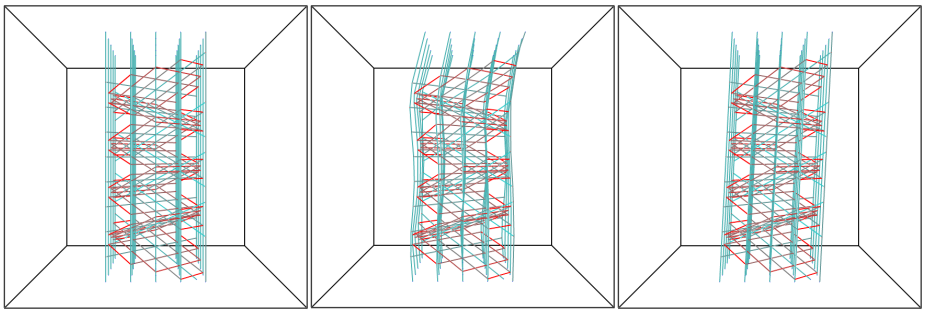

Fig. 4. Visualisations of one of the lattice based 3D networks, for the undisplaced *(left)*, displaced *(centre)* and affinely displaced *(right)* generations of the network where $\gamma = 0.05$.

The example seen in Figure 4 has an average coordination number of $z_c = 4.31$ with fibres of varied length, ℓ, radius $r = 0.01$, and a prescribed but irregular orientation. Given a shear strain $\gamma = 0.05$, the network is fixed in the plane $y = 0$, and sheared in the $y = 1$ plane in the positive x direction. Figure 4 *(left)* shows

the structure prior to any shear, Figure 4 *(centre)* shows the structure displaced after shearing, where the displacements are calculated using a direct solver. Figure 4 *(right)* shows the structure with every node displaced affinely. The total energy in this case is $E_{\text{aff}}^{\text{total}} = 5.0e^{-7}$. Comparing *(centre)* and *(right)*, we can see regions of the network in *(centre)* where bending is more favourable than affine displacement. The total energy here is $E^{\text{total}} = 1.4e^{-7}$, where bending energy $E^{\text{bend}} = 1.3e^{-7}$ is the main contribution.

5 Continued Work

Although lattice-based modelling can provide valuable insight into the mechanical properties of random fibre networks, truly representing real-world materials is still an issue. This will require a model with genuinely random orientation, using one of the two approaches for minimum distance calculation discussed in Section 2.5.

The size of the linear system becomes significant in 3D and parallel computing will be essential to model realistic volumes of material. We intend to use PETSc [1] to develop scalable tools for solving our systems, employing the block preconditioned iterative methods demonstrated in Section 4.1.

References

1. Balay, S., Abhyankar, S., Adams, M., Brown, J., Brune, P., Buschelman, K., Dalcin, L., Eijkhout, V., Gropp, W., Kaushik, D., Knepley, M., May, D., McInnes, L., Mills, R., Munson, T., Rupp, K., Sanan, P., Smith, B., Zampini, S., Zhang, H., Zhang, H.: PETSc Web page (2018), http://www.mcs.anl.gov/petsc
2. Broedersz, C., Mao, X., Lubensky, T., MacKintosh, F.: Criticality and isostaticity in fibre networks. Nature Physics **7**(12), 983–988 (2011)
3. Head, D., MacKintosh, F., Levine, A.: Nonuniversality of elastic exponents in random bond-bending networks. Phys. Rev. E **68**(2), 25101 (2003)
4. Head, D., Levine, A., MacKintosh, F.: Deformation of Cross-Linked Semiflexible Polymer Networks. Physical Review Letters **91**(10), 108102 (2003)
5. MacKintosh, F.: Elasticity and dynamics of cytoskeletal filaments and their networks. In: Soft condensed matter physics in molecular and cell biology, pp. 139–145. Taylor & Francis (2006)
6. Storm, C., Pastore, J., MacKintosh, F., Lubensky, T.C., Janmey, P.: Nonlinear elasticity in biological gels. Nature **435**(7039), 191 (2005)
7. Wilhelm, J., Frey, E.: Elasticity of Stiff Polymer Networks. Physical Review Letters **91**(10), 108103 (2003)